Bioactive Materials 9 (2022) 1–14

Contents lists available at ScienceDirect

Bioactive Materials

journal homepage: www.keaipublishing.com/en/journals/bioactive-materials

Bio-clickable mussel-inspired peptides improve titanium-based material osseointegration synergistically with immunopolarization-regulation

Jie Sun [a,1], Yingkang Huang [a,1], Huan Zhao [a,1], Junjie Niu [a], Xuwei Ling [a], Can Zhu [a], Lin Wang [a], Huilin Yang [a], Zhilu Yang [b,c,**], Guoqing Pan [d,***], Qin Shi [a,*]

[a] Department of Orthopaedics, The First Affiliated Hospital of Soochow University, Orthopaedic Institute of Soochow University, 899 Pinghai, Suzhou, Jiangsu, 215031, China
[b] Affiliated Dongguan Hospital, Southern Medical University, No. 3 Wandao Road, Dongguan, Guangdong, 523059, China
[c] Guangdong Provincial Key Laboratory of Shock and Microcirculation, No. 1023 Shatai Road, Guangzhou, Guangdong, 510080, China
[d] Institute for Advanced Materials, School of Materials Science and Engineering, Jiangsu University, 301 Xuefu Road, Zhenjiang, Jiangsu, 212013, China

ARTICLE INFO

Keywords:
Titanium implant
Clickable mussel-inspired peptide
Bio-orthogonal reaction
Osseointegration
Immunopolarization

ABSTRACT

Upon the osteoporotic condition, sluggish osteogenesis, excessive bone resorption, and chronic inflammation make the osseointegration of bioinert titanium (Ti) implants with surrounding bone tissues difficult, often lead to prosthesis loosening, bone collapse, and implant failure. In this study, we firstly designed clickable mussel-inspired peptides (DOPA-N3) and grafted them onto the surfaces of Ti materials through robust catechol-TiO_2 coordinative interactions. Then, two dibenzylcyclooctyne (DBCO)-capped bioactive peptides RGD and BMP-2 bioactive domain (BMP-2) were clicked onto the DOPA-N3-coated Ti material surfaces via bio-orthogonal reaction. We characterized the surface morphology and biocompatibility of the Ti substrates and optimized the osteogenic capacity of Ti surfaces through adjusting the ideal ratios of BMP-2/RGD at 3:1. *In vitro,* the dual-functionalized Ti substrates exhibited excellent promotion on adhesion and osteogenesis of mesenchymal stem cells (MSCs), and conspicuous immunopolarization-regulation to shift macrophages to alternative (M2) phenotypes and inhibit inflammation, as well as enhancement of osseointegration and mechanical stability in osteoporotic rats. In summary, our biomimetic surface modification strategy by bio-orthogonal reaction provided a convenient and feasible method to resolve the bioinertia and clinical complications of Ti-based implants, which was conducive to the long-term success of Ti implants, especially in the osteoporotic or inflammatory conditions.

1. Introduction

Titanium (Ti) is one of the most commonly used biomaterials in orthopedic, oral, and maxillofacial surgery, mainly attributed to its favorable mechanical properties, high biocompatibility as well as durability [1]. The application of threaded Ti-based implant technology has achieved excellent clinical outcomes. For example, dental Ti implants have been proved to be safe and effective in many patients. However, it is worth noting that implantation failure still occurs in the cases of osteoporosis, periodontitis, rheumatoid arthritis, diabetes mellitus, etc, mainly due to inadequate osteogenesis and feeble osseointegration [2,3]. Admittedly, the sluggish osteogenicity constantly observed in the edentulous and osteoporotic patients impairs the osseointegration of bare Ti implants. To make matters worse, the bioinertness of the bare Ti-based implants, especially in the upper threads, often causes macrophage and osteoclast activation, resulting in an inflammatory microenvironment (peri-implantitis) that inhibits osteogenesis and osseointegration, and subsequently cause implant failure [4,5].

As mentioned, surface properties of Ti-based implants and local microenvironment are the critical factors for rapid osteogenesis and osseointegration, as it determines the fate of osteogenesis-related cells

Peer review under responsibility of KeAi Communications Co., Ltd.
* Corresponding author.
** Corresponding author. Affiliated Dongguan Hospital, Southern Medical University, No. 3 Wandao Road, Dongguan, Guangdong, 523059, China.
*** Corresponding author.
E-mail addresses: zhiluyang1029@126.com (Z. Yang), panguoqing@ujs.edu.cn (G. Pan), shiqin@suda.edu.cn (Q. Shi).
[1] These authors contributed equally to this work.

https://doi.org/10.1016/j.bioactmat.2021.10.003
Received 30 July 2021; Received in revised form 22 September 2021; Accepted 3 October 2021
Available online 7 October 2021

[1,6]. Hence, to ensure long-term success upon the challenging clinical conditions, it is necessary to modify the surface of Ti-based implants to endow them with the desired bioactivities [7,8]. The primary goal of Ti-based implants modification is to improve the osseous tissue compatibility, suppress peri-implantitis, as well as facilitate early osteogenesis and osseointegration, and finally achieve long-term success [9]. For these purposes, many bioactive molecules, including extracellular matrix proteins and osteoinductive factors, were decorated on the surface of Ti-based implants to enhance the adhesion and differentiation of osteoprogenitors and modulate the local inflammation microenvironment [9,10]. For example, RGD peptide or osteogenic growth peptide (OGP)-decorated Ti-based implants could significantly enhance osteogenesis and osteodifferentiation [11–13].

Many methods have been developed to decorate Ti-based implant surfaces with bioactive molecules in the past decades: sputter-deposition, electrophoretic deposition, sol-gel coating, and plasma spraying or chemical crosslinking, and so on [14–17]. However, traditional surface modification strategies mainly rely on covalent bonding to graft bioactive molecules onto the surfaces of Ti-based implants, which will inevitably impair the active epitopes of the biomolecules. Moreover, these methods usually involve tedious chemical reactions and intricate procedures, which are less maneuverable, reproducible, and controllable for clinical application [8]. Nevertheless, physical adsorption often results in drug exfoliation due to weak non-covalent bonds and is unable to play long-term bioactivity [5,18]. In addition, the long-term effects of earlier surface modification strategies were far from ideal, mainly due to the monotonicity of surface bioactivity rarely consider the complexity of challenging conditions [19]. Therefore, to improve the long-term osseointegration of Ti-based implants, simple, flexible, and feasible modification strategies need to be considered.

Comfortingly, the development of biomimetic technologies shows inherent superiority as they attempt to integrate a single component or the combination of these components on the surface of the implant in a flexible and convenient way [9,20,21]. These future trends involve changes in surface compositions that promote cell adhesion, biomimetic coatings for enhancing osteoconduction, and accelerating bone healing around implants [7,9,20]. By looking for inspiration from nature, Mussel-inspired adhesion has been used to functionalize the surface of Ti-based implants [21–23]. The molecular mechanism of the mussel-inspired surface modification strategy is derived from the adhesion protein secreted by mussels and its repeated catechol amino acid (3, 4-dihydroxy-L-phenylalanine, DOPA) can stably adhere to almost diverse substrates in aqueous solutions via covalent and non-covalent bonds [22–25]. However, DOPA-based biomolecular conjugations mainly depend on covalent reactions, which may destroy the bioactivities of biomolecules. Therefore, it is urgent to improve the current mussel-inspired surface modification strategies in orthopedics, oral and maxillofacial surgery to cope with the challenging clinical conditions.

Fortunately, the development of bio-orthogonal reactions provides us with a new idea, a kind of click chemical reaction that can occur under physiological conditions [26]. Due to the advantages of mild and straight forward reaction conditions, fast rate, specificity, and biocompatibility, expanding the application of click chemistry in implant surface modification has become a research hotspot [27,28].

Based on the above considerations, the multi-functionalized Ti implants reported in this study decorated with two bioactive peptides: MSCs-anchoring peptide-RGD and osteoinductive peptide-BMP-2, via an easy-to-perform, two-step surface modification strategy could satisfy all requirements. The motivation for the combined use of RGD and BMP-2 mainly comes from the fact that in addition to promoting MSCs adhesion, pieces of evidences have indicated that RGD-integrin interaction could also enhance the osteoinductivity of BMP-2 via increasing the phosphorylation of Smad1/5/8, thus synergistically accelerating the osteodifferentiation of MSCs [29–32]. Furthermore, BMP-2 protein can also regulate the transition of macrophages from the pro-inflammatory M1phenotype to the anti-inflammatory M2 phenotype [33–36]. Previous studies by us and others have demonstrated that M2 macrophages can inhibit inflammation and osteoclast differentiation by secreting anti-inflammatory factor IL-10, and secrete VEGF-A and TGF-β to promote angiogenesis and differentiation of MSC into osteoblasts, so as to promote osteogenesis [33–37].

Here, we decorated the Ti-based implants through the combination of mussel-inspired peptide adhesion and bio-orthogonal click chemistry. First, we loaded a clickable mussel-inspired peptide with catechol groups and Azido (DOPA-Azido) onto the Ti-based material surfaces via imitating the molecular structure of mussel foot proteins (Mfps). Like Mfps, the mussel-inspired peptide (DOPA) could stably bind to the TiO_2 film of Ti-based materials through spontaneous metal-catechol coordination [6]. After that, two bioactive peptides, RGD and BMP-2, capped with dibenzylcyclooctyne (DBCO, the click reaction group of Azido), were covalently bound to the Azido group through bio-orthogonal click reaction, thus realizing the dual-functionalized modification of Ti implant surfaces (Scheme 1). Our results confirmed that, at the optimal feeding ratio of BMP-2/RGD at 3:1, the dual-functionalized Ti material could enhance the adhesion and osteodifferentiation of MSCs, inhibit inflammation, and ultimately enhanced the osteogenesis and osseointegration at the bone-implant interface in osteoporotic rats.

Due to the rapid, thorough, and specific advantages of the bio-orthogonal reaction, the Ti-based prosthesis could be endowed with adjustable multi-function (i.e., anchoring, osteoinductivity, and immunomodulatory capability, etc.) through a feeding-dependent co-grafting process. We expected that the surface modification strategy proposed in this study could provide a simple, flexible, and convenient method for the functionalization of Ti-based implants. Such functionalized Ti-based implants could conquer the challenging clinical microenvironment, such as osteoporosis, periodontosis, peri-implantitis, diabetes mellitus, and thereby ultimately accelerating osteogenesis and osseointegration. Therefore, it has a wide range of practical application values in orthopedics, oral and maxillofacial surgery.

2. Materials and methods

2.1. Synthesis of the biomimetic peptides

The mussel-inspired adhesive peptide capped with Azido ($(DOPA)_4$-PEG_5-Azido, DOPA-Azido): Ac-(DOPA)-Gly-(DOPA)-(Lys-PEG_5-Azido)-(DOPA)-Gly-(DOPA)-

COOH was synthesized as our previous studies described [24,38]. Briefly, Fmoc-DOPA (acetonide)-OH (1 mmol) (Okeanos Tech Co., Ltd., China), N,N-Diisopropylethylamine (DIPEA, 4 mmol), and 2-chlorotrityl chloride resin (1.6 g, 1.6 mmol, Alfa Aesar, China) was dissolved in 20 mL of dichloromethane (DCM) and then shaken at room temperature (about 25 °C) for 4 h. After washing, the Fmoc-DOPA-grafted resin was covered with methanol using DCM/MeOH/DIPEA (15:2:1). Subsequently, to uncover the amino group, the Fmoc group was easily removed by 20% piperidine in N-methyl-2-pyrrolidone (NMP). Then, Fmoc-Gly-DOPA-grafted resin was obtained by adding amino acids using Fmoc-Gly-OH/BOP/DIPEA (1.5:1.5:1.5, mmol) in NMP. After that, Fmoc-DOPA (acetone)-OH, Fmoc-Lys(Dde)-OH, and Fmoc-Gly-OH were grafted onto the resin in turn to obtain Fmoc-(DOPA)-Gly-(DOPA)-(Lys (Boc))-(DOPA)-Gly-(DOPA)-grafted resin. The Dde-protected amine groups in Lys were activated by 20% hydrazine hydrate/N,Ndimethylformamide (DMF) and then reacted with Azido--PEG_5-COOH/BOP/DIPEA (1.5:1.5:1.5, mmol) in NMP to acquire the Fmoc-(DOPA)-Gly-(DOPA)-(Lys-PEG5-Azido)-(DOPA)-Gly- (DOPA)--grafted resin. After the Fmoc group was wiped from the final amino acid, the amino group was covered with acetyl group using Ac_2O/DIPEA/NMP (1:4:40). Subsequently, 2% trifluoroacetic acid (TFA) was used to cut off the protected peptide acid from the resin. Finally, the clickable mussel-inspired adhesive peptide ($(DOPA)_4$-PEG_5-Azido) was obtained through high-performance liquid chromatography (HPLC)

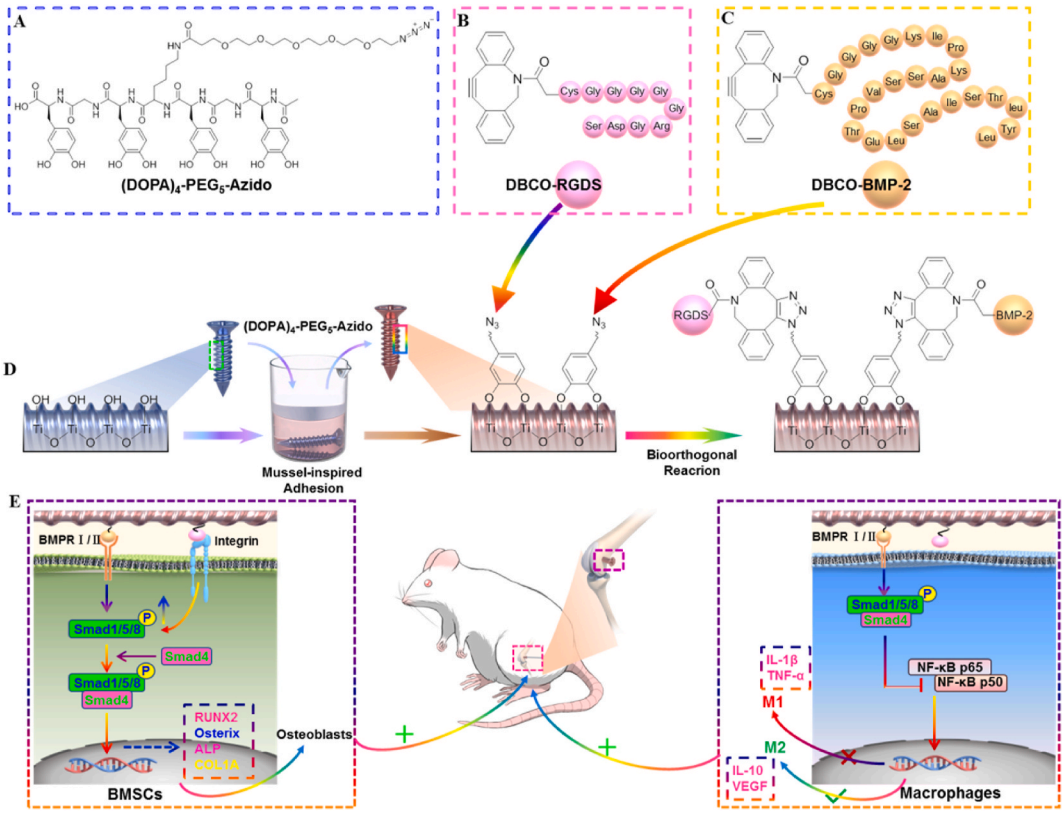

Scheme 1. Schematic diagram of the biomimetic modification of Ti-based implants. (A) Molecular structure of the clickable mussel-inspired peptide ($(DOPA)_4$-PEG_5-Azido). (B) Structure of DBCO-capped RGD peptide. (C) Structure of DBCO-capped BMP-2 peptide. (D) Mussel-inspired adhesion and bio-orthogonal reactions are combined for surface modification of Ti-based implants. (E) Dual-functionalized Ti-based implants can enhance osteogenesis and osseointegration through promoting MSCs adhesion and osteodifferentiation, as well as modulate macrophage polarization in the osteoporotic rats.

purification.

DBCO-conjugated RGD (DBCO-RGD) and BMP-2 (DBCO-BMP-2) peptides were synthesized as the following procedure [26]. Firstly, RGD (Arg-Gly-Asp-Ser) and BMP-2 (Lys-Ile-Pro-Lys-Ala-Ser-Ser-Val--Pro-Thr-Glu-Leu-Ser-Ala-Ile-Ser-Thr-Leu- Tyr-Leu) peptide backbones were synthesized with an additional flexible linker (Gly_4-Cys), respectively. Then, the thiol group of Cys was capped with Dibenzocyclooctyne-maleimide (DBCO-MAL) to obtain the Fmoc-DBCO-Cys-Gly-

Gly-Gly-Gly-Arg-Gly-Asp-Ser (DBCO-RGD) or Fmoc-DBCO-Cys-Gly-Gly-Gly-Gly

-Lys-Ile-Pro-Lys-Ala-Ser-Ser-Val-Pro-Thr-Glu- Leu-Ser-Ala-Ile-Ser-Thr-Leu-Tyr-

Leu (DBCO-BMP-2)-grafted resin. Subsequently, the peptides were eluted from the resin using 2% TFA in DCM solution and purified by HPLC.

2.2. Purification and characterization of the synthetic peptides

The purification of the synthesized peptides was performed on an Agilent HPLC system using a Kromasil 100-5C18 column (5 μm, 4.6 × 250 mm, column temperature 25 °C) at a linear flow rate of 1 mL/min 0.1% TFA in water (Buffer A) and 0.1% TFA in acetonitrile (Buffer B) were used as mobile phases. The volume of injection was 10 μL and running time was 11 min. After purification, the synthetic peptides were characterized by electrospray ionization mass spectrometry (ESI-MS) to confirm their molecular weights at a flow rate of 0.2 mL/min (Buffer: 75% Acetonitrile (ACN)/24.5%H_2O/0.5%Ac; run time: 1 min).

2.3. Peptides coating and characterization of the modified Ti substrates

In this study, TiO_2-coated quartz plates were used for *in vitro* tests. All peptides were dissolved in phosphate-buffered solution (PBS) and purged with nitrogen for 15 min at room temperature. Firstly, TiO_2-coated quartz plates were immersed in $(DOPA)_4$-PEG_5-Azido (DOPA-Azido) solution for 30 min at a final concentration of 0.01 mg/mL for the mussel-inspired peptide adhesion. Then, DOPA-Azido-coated TiO_2 substrates were incubated with DBCO-RGD, DBCO-BMP-2, or their mixed peptides solution at a total concentration of 0.1 mM with different feeding ratios for 10 min. After that, the plates were rinsed thoroughly with deionized water to discard dissociative peptides and dried for further use. To directly demonstrate that DBCO-capped molecules could bind onto DOPA-Azido-coated TiO_2 surfaces via bio-orthogonal reaction, DOPA-Azido-coated TiO_2 plates were incubated with Alexa Fluor-488-conjugated DBCO (DBCO-AF_{488}, Sigma, Germany) for 15 min at room temperature. After washing, the TiO_2 plates were observed and photographed with a fluorescence microscope (Carl Zeiss, Germany).

The chemical compositions of the surfaces of peptide-coated TiO_2 substrates were analyzed by the X-ray photoelectron spectroscopy (XPS) instrument (ESCALAB MK II X-ray photoelectron spectrometer, VG Scientific). The X-ray source worked under a pressure of 12kv, 15 mA, 3 × 10^{-7} Pa, and the graphitic carbon peak (285 eV) was set as the reference for charge calibration.

The KRÜSS DSA25 contact angle equipment (DSA25S, America) was used to evaluate the hydrophilicity of the peptides-coated surfaces. At room temperature, the sessile droplet shapes of deionized water (5 μL) on different surfaces were imaged, and the static water contact angle (WCA) was quantified by DSA 1.8 software. In addition, the roughness and topology of different modified surfaces were acquired by the atom force microscope (AFM, Bruker, Germany).

2.4. Isolation of bone-marrow mesenchymal stem cells (BMSCs) from osteoporotic rats

All the animal procedures were licenced by the Animal Care and Use Committee of Soochow University, and abided by the Guide for the Care and Use of Laboratory Animal of the National Institute of Health (NIH).

In order to truly reflect the biological properties of Ti-based implants under challenging clinical conditions, bone-marrow mesenchymal stem cells (BMSCs) used in the *in vitro* study were derived from the osteoporotic rats. Therefore, we first established the osteoporotic rat (OP) models via ovariectomy (OVX) according to our previous study described [25].

At 8 weeks post the surgery, the rats were scanned by micro CT (SkyScan1176, Belgium), and then bone mass analysis was performed to determine the occurrence of osteoporosis. Then, BMSCs were isolated from the bone marrow of osteoporotic female rats as the previous study described [25].

2.5. Adhesion and proliferation of BMSCs

BMSCs adhesion test was performed by seeding 1×10^5 cells in a 24-well cell plate on the different modified TiO_2-coated plates with serum-free medium. The cell plates were shaken with a rotating speed of 80 rpm in a cell culture chamber to more realistically simulate the flow of body fluids *in vivo*. After incubation for 3 h, all the samples were washed with PBS, fixed in 4% paraformaldehyde, and stained with fluorescein-5-isothiocyanate (FITC)-conjugated Phalloidin. Adhered cells were observed by an upright fluorescence microscope and analyzed by the Image J software (NIH, USA).

In addition, the same numbers of BMSCs were seeded on the corresponding substrates using the Dulbecco's modified Eagle's medium (DMEM) complete medium for 72 h. Then, cell proliferation was analyzed using the Cell Counting Kit-8 (CCK-8; Beyotime, China) according to the manufacture's instruction. Moreover, Live/Dead cell staining (Invitrogen, USA) and lactate dehydrogenase (LDH) detection kit (Beyotime, China) was used to evaluate the viability of BMSCs and the biocompatibility of different modified TiO_2 substrates. The experiment was divided into six groups: untreated bare TiO_2 substrates (TiO_2), only DOPA-Azido-coated substrates (DOPA), DOPA-coated substrates grafted with DBCO-BMP-2 alone (4:0), DOPA-coated substrates grafted with different feeding ratios of DBCO-BMP-2 and DBCO-RGD peptides (BMP-2:RGD = 3:1 and 2:2, respectively) and DOPA-coated substrates grafted with DBCO-RGD alone (0:4).

2.6. Osteogenic differentiation of BMSCs in vitro

To test the osteoinductive activity of different modified TiO_2 substrates, 1×10^5 BMSCs were seeded on the corresponding substrates with osteoinductive DEME medium, respectively, containing 50 μg/mL L-ascorbic acid (Sigma-Aldrich, Germany), 100 nM dexamethasone (Sigma-Aldrich, Germany), and 10 mM β-glycerol phosphate (Sigma-Aldrich, Germany), which was replaced every 3 days.

After 24 h, Western blotting (WB) was performed to detect the expression of BMP-2 receptor (BMPR)/Smad signaling pathway-related proteins in BMSCs, including BMPRII, Smad1/5/8 and Smad4, and BMP-2. Briefly, the proteins extracted from BMSCs were separated and transferred onto the poly-vinylidene difluoride membranes (PVDF). The membranes were incubated with the primary antibodies against BMPRII (Abcam, UK), Smad1/5/8 (Millipore, Germany), Smad4 (Abcam, UK), and β-actin (Abcam, UK), and then washed and further incubated with goat anti-rabbit or anti-mouse IgG second antibodies (Abcam, UK). The protein bands were detected with a gel imaging system (Bio-Rad, USA), and the relative intensity of the protein was quantified by ImageJ software.

Quantitative-PCR (qPCR) was performed to detect the expression of osteodifferentiation-related genes after 3 (Runt-related transcription factor 2 (Runx2), Osterix) and 7 days (Alkaline phosphatase (ALP), collagen1A1 (COL1A1)), respectively. Gene expression levels were normalized to β-actin expression and analyzed according to the comparative Ct ($2^{-\Delta\Delta Ct}$) method. The primers for all genes were purchased from GeneWIZ Lt.co (China), and their sequences were listed in Supplementary Table 1(Table S1).

After 7 days, ALP staining and quantitative analysis were performed to evaluate the osteodifferentiation of BMSCs using the BCIP/NBT Alkaline Phosphatase Color Development Kit (Beyotime, China) and ALP Assay Kit (Biyuntian, China) according to the manufacturer's instructions. Subsequently, on day 14, alizarin red staining (ARS) was employed (Solarbio, China) to examine the calcium deposition. After observing and photographing with a microscope, the mineralization nodules were dissolved and extracted with 5% perchloric acid at room temperature for 20 min, and the absorbance was measured at 490 nm by a microplate reader (Gene, USA).

2.7. Macrophage polarization in vitro and in vivo

The osteoporotic rats-derived bone marrow cells were cultured with Modified Eagle's Medium (MEM) supplemented with 10% FBS overnight, and then the non-adherent cells were harvested and cultured with MEM complete medium containing 10 ng/mL Macrophage-Colony Stimulating Factor (M-CSF; Pepreotech, USA) for 72 h to obtain the bone-marrow derived mononuclear cells (BMMs). Subsequently, BMMs were seeded on the different modified TiO_2 substrates and cultured in conditions that mimic an M1 pro-inflammatory environment (containing 50 ng/mL Lipopolysaccharides (LPS, Sigma-Aldrich, USA) and 50 ng/mL interferon-γ (IFN-γ, Pepreotech, USA). In order to simulate the low inflammatory state under osteoporotic conditions, the concentration of cytokines used in this section was half of the standard induction medium. After stimulation for 24 h, WB was performed to detect the expression of NF-κB signaling pathway-related proteins, including phosphorylated p65 (p-p65) and inhibitor of nuclear factor κ B (*p*-IκB), and semi-quantitative analysis by ImageJ software.

After 5 days, the cells and supernatant were collected. First, fluorescence-activated cell sorter (FACS) was performed to detect the surface markers of polarized macrophages. Briefly, the cells were incubated with the FITC-conjugated anti-CD68, allophycocyanin (APC)-conjugated anti-CD86 and CD206 antibodies (eBioscience, USA) at 4 °C for 30 min to confirm M1 ($CD68^+CD86^+$) and M2 ($CD68^+CD206^+$) phenotype. The cells were assayed by a flow cytometer (FCM) AriaII, BD), and the results were analyzed by the FlowJo V10 software. Second, the prepared supernatant was used to detect the cytokines secreted by M1 (IL-1β, TNF-α) and M2 (IL-10, VEGF) macrophages using enzyme linked immunosorbent assay (ELISA) kit (BlueGene, China) according to the manufacturer's instructions. In addition, qPCR was performed to detect the mRNA expression of M1 and M2 phenotype-related genes (iNOS, TNF-α, and IL1β). The primer sequences were summarized in Table S1.

Subsequently, the TiO_2 substrates were subcutaneously implanted into the osteoporotic rats to study their regulatory effects on macrophage polarization. At 5 days after implantation, the samples were harvested for immunofluorescence staining as the following procedures. Briefly, the samples were fixed, blocked, and then incubated with FITC-conjugated anti-CD68 and APC-conjugated anti-CD86 antibodies (M1) or APC-conjugated anti-C206 antibodies (M2) at 4 °C overnight, respectively. After washing, the sheets were mounted with ProLongGold Antifade Mountant containing diamidino-phenyl-indole (DAPI) (Invitrogen, USA) and coverslips, and then examined by a confocal laser scanning microscope (Carl Zeiss, Germany). The area of double-positive cells was analyzed by ImageJ software. According to the most superior effects of BMSCs adhesion and differentiation experiments, they were divided into four groups: TiO_2, DOPA-coated substrates grafted with DBCO-BMP-2 alone (BMP-2), DOPA-coated substrates grafted with DBCO-RGD alone (RGD), and DOPA-coated substrates grafted with

DBCO-BMP-2 and DBCO-RGD at the feeding ratio of 3:1 (RGD+BMP-2).

2.8. Ti screws implantation

We further investigated the effects of biomimetic peptide-modified Ti-based implants on osseointegration under challenging clinical conditions. Briefly, the prepared osteoporotic rats (n = 24, 6/group) were anesthetized by intraperitoneal injection of sodium pentobarbital (1 mL/kg) and fixed in the lateral position. After the surgical sites were shaved and disinfected, the skin, fascia, and periosteum were incised sequentially to expose the lateral condyle in the distal femurs. Subsequently, a low-speed electric drill mounted with a 1 mm Kirschner wire was used to create a channel deep into the medullary cavity in the femoral condyle, and then different modified screws were implanted into the bone manually using a screwdriver. The incisions were sutured layer by layer with absorbable sutures, and the animals were intraperitoneally injected with penicillin for 7 days.

2.9. Micro-CT scanning

After 8 w of implantation, the implanted Ti screws with the femoral condyles as a whole were harvested, and micro-computerized tomography (micro-CT) scanning (SkyScan1176, Belgium) was performed. The volume of interest (VOI) included the trabecular compartment between the outer diameter and the inner diameter of the screws longitudinal axis. More precisely, the VOI was chosen in an axisymmetric cuboid along the longitudinal axis of the screw, the top view of which was a rectangular plane (0.9 × 1.8 mm) with a depth of 6 mm. After scanning, three-dimensional (3D) digital image reconstruction was carried out using the supporting analysis software. Then the percentage bone volume (BV) among tissue volume (TV) (%, BV/TV), trabecular number (Tb.N), trabecular thickness (Tb.Th), trabecular bone pattern factor (Tb.Pf), and trabecular separation (Tb.Sp) within VOI were analyzed.

2.10. Histomorphometric analysis

Following micro-CT scanning, histological staining and quantitative analysis were performed to evaluate the osteogenesis and osseointegration on the Ti screws surfaces. Briefly, all samples were fixed with paraformaldehyde, washed with water, dehydrated with ethanol and transparent with xylene, and then embedded in poly (methyl methacrylate). The embedded blocks were cut into 300 μm-thick slices along the longitudinal axis and the implantation center using a hard tissue slicer (EXAKT 300CP) and then ground into 10 μm-thick slices with a Grinding System (EXAKT 400 CS). Then, the samples were stained with toluidine blue, and the images were acquired by an optical microscope (OLYMPUS BX43). The bone-implant contact (BIC, the percentage of implant circumference in direct contact with bone tissue in the threaded area) was calculated using BIOQUANT software (OSTEO 2016 system).

2.11. Biomechanical analysis

All the specimens were wrapped with gauze and soaked in saline at 4 °C before the pull-out testing. The samples were mounted on an Instron E10000 (Instron, MA, USA) equipped with a 500 N gauge. A steel plate (1 mm thick) with a 5 mm diameter hole was mounted on the resin plate to stabilize the specimens, and a customized clip was used to connect the cap of the screws and the jack of the testing machine [24]. The screws were pulled out from the bone at a displacement rate of 1 mm/min until they were completely separated, and the maximum failure load was recorded.

2.12. Statistical analysis

All data in this study were analyzed by SPSS 17.0 software and presented as mean ± standard deviation (SD). One way or two-way analysis of variance (ANOVA), followed by Tukey's post-analysis to determine the significant difference. $p < 0.05$ are considered to be the significant differences.

3. Results and discussion

3.1. Synthesis and identification of peptides

To simulate the adhesion of catecholic amino acid onto the TiO_2 substrates, the clickable mussel-inspired peptide ($(DOPA)_4$-PEG_5-Azido) was prepared by solid-phase peptide synthesis. Based on our previous studies [24,26,39,40], we improved the orientation of catechol to enhance the adhesion strength and efficiency of $(DOPA)_4$-PEG_5-Azido (DOPA) on the surface of TiO_2 substrates. Moreover, to avoid affecting the mussel-inspired peptide adhesion onto the TiO_2 substrates and subsequent clickable reaction, four DOPAs were separated by a flexible amino acid (Gly) and PEG-linked Azido to obtain a clickable mussel type adhesion peptide: Ac-(DOPA)-Gly-(DOPA)-(Lys-PEG_5-Azido)-(DOPA)--Gly-(DOPA)-COOH (Scheme 1A). As two critical factors for osteogenesis, RGD and BMP-2 peptides were conjugated with DBCO through N-hydroxysuccinimide and maleimide-thiol coupling, respectively (Scheme 1B and C). Thus, the TiO_2 substrates grafted with DOPA-Azido could bind DBCO-RGD and DBCO-BMP-2 through the click reaction, endowing them with dual-functionalization (Scheme 1D and E).

After purification by HPLC (Supplementary Fig. S1A), the three synthesized peptides were then characterized with ESI-MS. The monoisotopic mass $[M+H]^+$ of $(DOPA)_4$-PEG_5-Azido and DBCO-RGD, and $[M+2H]^{2+}$ of DBCO-BMP-2 were measured at 1336.8, 1250.1 and 1439.8 Da, consisting with their theoretical molecular weight 1336.4, 1249.6 and 2877.3,respectively (Fig. S1B). These results confirmed that the successful synthesis of the Azido-capped mussel-inspired peptide ($(DOPA)_4$-PEG_5-Azido) and DBCO-conjugated bioactive peptides (DBCO-RGD and DBCO-BMP-2).

3.2. Characterization of biomimetic peptides-grafted Ti substrates

Our previous studies had shown that multivalent catechol-capped moieties could rapidly and stably bind onto the TiO_2 substrates via the coordination covalent bond [24,28,30]. Therefore, DBCO-conjugated moieties should be able to be grafted onto the DOPA-Azido-coated TiO_2 surface via bio-orthogonal reaction. As shown in Fig. 1A, green fluorescence could only be observed on the TiO_2 surfaces treated by DOPA-Azido and DBCO-AF_{488} successively, indicating that DOPA-Azido could successfully adhere to the TiO_2 surface and rapidly bind the DBCO-conjugated moieties through bio-orthogonal conjugation.

Surface elemental compositions of TiO_2 substrates grafted with different peptides were characterized by XPS. A remarkable enhancement in N 1s signal on the DOPA-Azido (DOPA) coated and DBCO-RGD or DBCO-BMP-2 grafted on DOPA-Azido coated surfaces, which was consistent with the content of amino in the corresponding peptide, respectively (Fig. 1B). Quantitative data showed that the atomic ratio of N/Ti increased from 0.09 (bare TiO_2) to nearly 0.32 (DBCO-RGD-grafted) and 1.37 (DBCO-BMP-2-grafted), respectively (Table S2). These results demonstrated that the mussel-inspired peptide and DBCO-coupled peptides were successively grafted onto the surfaces of the TiO_2 substrate. By adjusting the types and feeding ratio of peptides could achieve the functional diversities and flexibilities of the surface modification of Ti-based implants.

According to the results of XPS, we further examined the hydrophilicity and micromorphology of the TiO_2 substrates. As shown in Fig. 1C–E, co-grafted surfaces had better hydrophilicity and rough surface morphology, which was conducive to cell adhesion and stretching [41]. Surface topography and roughness are critical for the adhesion of osteoblasts and the interlocking between bone and implant, thus enhancing osseointegration compared to the smooth surface. In

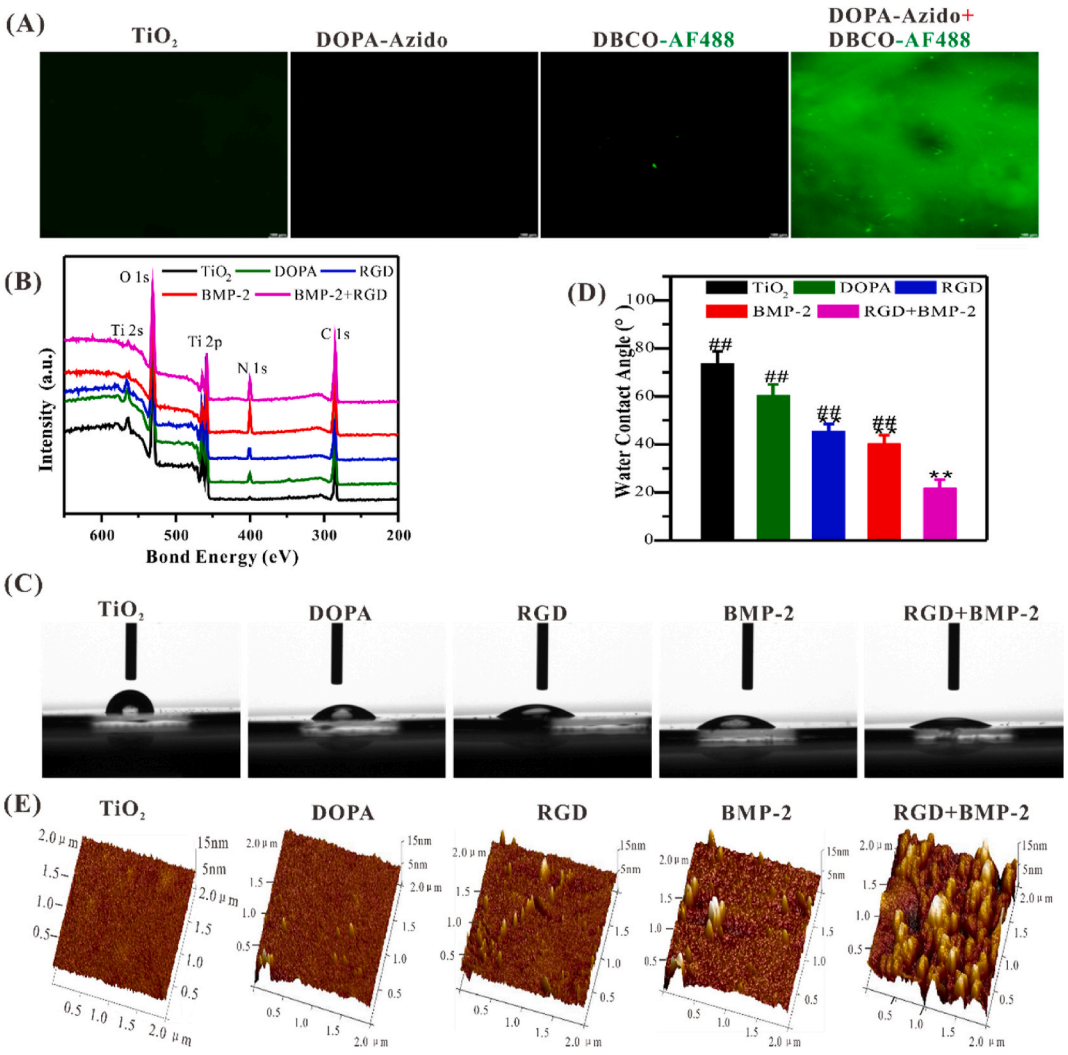

Fig. 1. Characterization of biomimetic peptides-modified TiO_2 surfaces. (A) Representative fluorescence images showed that the clickable DOPA-Adizo could successfully adhere onto the TiO_2 substrate and bind to DBCO-capped moieties. Scale bar = 100 μm. (B) Elemental composition changes on different modified TiO_2 surfaces. (C, D) Representative images of static water-contact angle and quantitative analysis. (E) AFM images of different-treated TiO2 surface. Significant differences were indicated by *p < 0.05 or **p < 0.01 compared with bare TiO2 surface, and #p < 0.05 or ##p < 0.01 compared with the DBCO-BMP-2/DBCO-RGD co-grafted (3:1) surfaces (n = 3).

addition, the hydrophilic surface can maintain the conformation and function of the protein, thereby promoting cell adhesion and differentiation [42,43].

3.3. Biocompatibility and cell-anchoring ability of different TiO_2 surfaces

The functionalized Ti-based implants with cell capturing and osteoinductivity are very critical for the early osteogenesis and osseointegration *in vivo*. To more authentically simulate clinically challenging conditions, BMSCs derived from osteoporotic rats (OP-rats) were used to evaluate the cell-anchoring ability, osteoinductivity, and biocompatibility of the TiO_2 substrates with different grafting ratios of DBCO-RGD and DBCO-BMP-2 *in vitro*. The bare (TiO_2 group) and $(DOPA)_4$-PEG_5-Azido-coated TiO_2 substrates (DOPA group) were used as controls. Here, we first assessed the biocompatibility of different modified TiO_2 surfaces via Live/Dead cell staining and measurement of LDH released from the damaged cells. There was no statistical difference in the proportion of live and dead cells in all groups (Fig. 2A and C), however, LDH showed all the peptide-grafted substrates displayed lower cytotoxicity compared to the bare TiO_2 substrates, especial co-grafted ones, indicating peptides-decoration could improve the biocompatibility of TiO_2 substrates.

For BMSCs anchoring experiments, all TiO_2 substrates were placed on a horizontal shaker with a rotational speed of 80 rpm in the cell culture chamber to more realistically imitate the humoral flow *in vivo* environment. Considering the inevitable influence of serum components on non-specific cell adhesion, medium without serum were used to assess specific BMSCs adhesion on the TiO_2 substrates. After 3 h of incubation, the adherent BMSCs was examined by FITC-conjugated Phalloidine staining (Fig. 2B and D). Although there were BMSCs adhesion on all the TiO_2 substrates, the co-grafted groups with higher DBCO-RGD feeding ratios (i.e., 1:3, 2:2 and 0:4) exhibited stronger BMSC-anchoring ability compared to the others. With the increased feeding ratio of DBCO-RGD, the number of adherent cells also increased. As expected, only a small number of cells were observed in the RGD and BMP-2-free groups (i.e., TiO_2 and DOPA) under serum-free conditions. The serum contains proteins that could be adsorbed on the surface and induce non-specific cell adhesion. Thus serum-free condition is conducive to confirm the specific interactions between RGD motifs and integrin $\alpha v\beta 3$, as well as BMP-2 and BMP receptors (BMPRs).

It's worth noting that there was also a significant enhancement of BMSCs adhesion on the only DBCO-BMP-2-grafted surfaces (4:0) compared to the controls. More importantly, at the feeding ratios (BMP-2/RGD) of 3:1 and 2:2, BMSCs adhesion number of co-grafted TiO_2

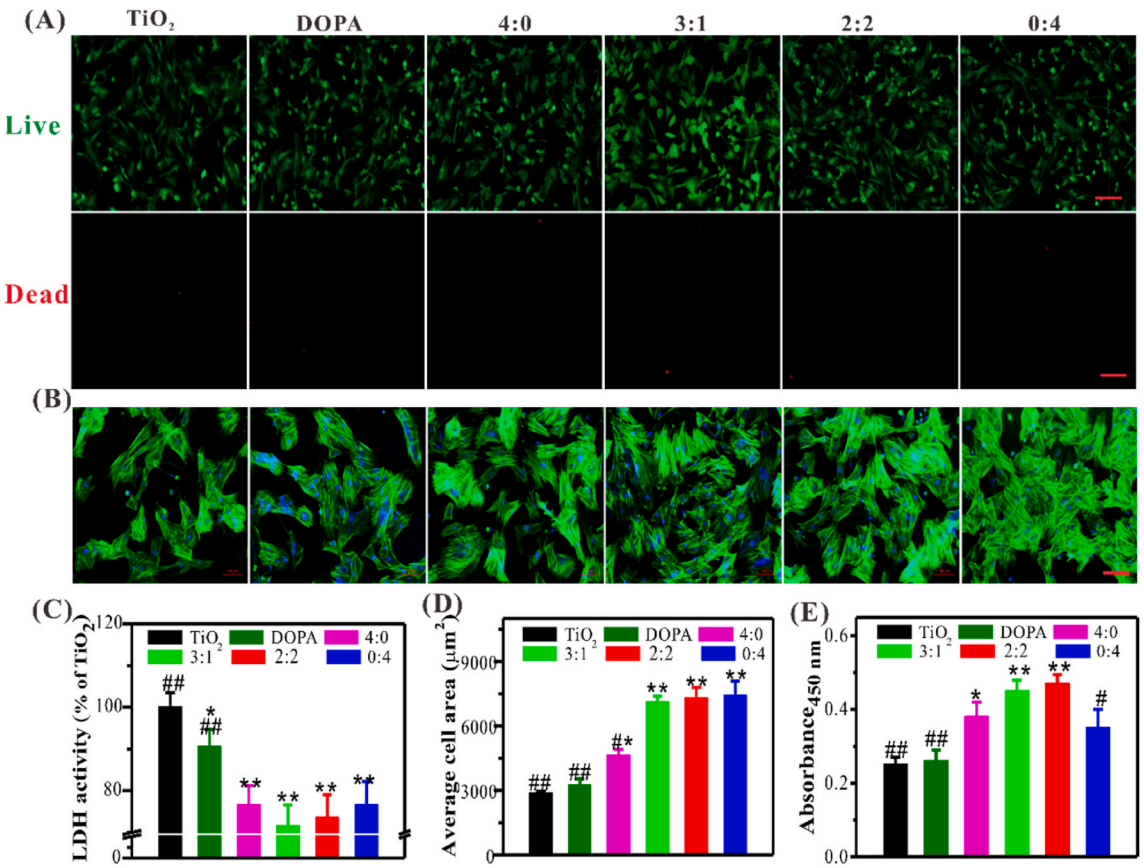

Fig. 2. Biocompatibility and cell anchoring capacity of different modified TiO2 substrates. (A) Representative images of Live/Dead cell staining (Scale bar = 100 μm). (B) The morphologies of adherent BMSCs after 3 h of culture in FBS-free medium on different surfaces (Blue, DAPI; Green, FITC-conjugated phalloidin) (Scale bar = 100 μm). (C) Quantification of LDH. (D) Quantification of adhered cells. (E) The proliferation of BMSCs. Significant differences were indicated by *p < 0.05 or **p < 0.01 compared with bare TiO2 surfaces, and #p < 0.05 or ##p < 0.01 compared with the DBCO-BMP-2/DBCO-RGD (3:1) co-grafted surfaces (n = 3). (For interpretation of the references to colour in this figure legend, the reader is referred to the Web version of this article.)

substrates showed no significant difference compared to full DBCO-RGD-grafted ones (0:4), which might be mainly owing to the interaction between BMP-2 and BMPRs could also enhance cell adhesion. These findings together confirmed the specific peptides-mediated cell adhesion on the co-grafted surface. Furthermore, BMSCs on the BMP-2-containing surfaces (4:0, 3:1, and 2:2) exhibited the active spreading morphology, which was conducive to proliferation and osteodifferentiation. As shown in Fig. 2E, all the peptide-grafted substrates showed a significant increase in cell proliferation after culture for 3 days as compared to the control groups. Moreover, the BMP-2 and RGD co-grafted groups (i.e., 3:1 and 2:2) showed obviously synergistic effects. To sum up, RGD plays a major role in BMSCs adhesion, which is different from non-specific physical adsorption [24,25]. Nevertheless, BMP-2 plays an incomparable role in osteogenic differentiation [29]. At the feeding ratio of 3:1, the DBCO-BMP-2/DBCO-RGD co-grafted TiO_2 surfaces exhibited improved biocompatibility, cell adhesion and proliferation. Therefore, by adjusting the feeding ratio of DBCO-BMP-2 and DBCO-RGD, they can synergistically enhance the adhesion and osteodifferentiation of BMSCs, which is of great significance for early osteogenesis and osseointegration *in vivo*.

3.4. BMSCs osteodifferentiation on different TiO_2 surfaces

We further investigated the *in vitro* osteodifferentiation of BMSCs from osteoporotic rats on different peptides-modified surfaces. ALP staining and activity analysis were first carried out after 7 days of culture in the osteoinductive medium, an early marker of osteodifferentiation. As demonstrated in Fig. 3A and B, RGD mono-grafted surface (i.e., 0:4) could enhance BMSCs adhesion, whereas no significant enhancement was found in osetodifferentiation compared to the control groups (i.e., TiO_2 and DOPA). In contrast, upon the addition of BMP-2 (i.e., 4:0, 3:1 and 2:2), osteodifferentiation enhanced remarkable. More importantly, co-grated surfaces could produce higher ALP activity than the controls (i.e., TiO_2 and DOPA) and mono-grafted ones (i.e., 4:0 and 0:4), which may be mainly attributed to the synergistic effect of cell adhesive peptide RGD and osteoinductive BMP-2 peptide. Notably, ALP activity of the group with a feeding ratio of 3:1 (BMP-2/RGD) was the highest, nearly 1.4 and 1.7-fold enhancement as compared to the group with that of 4:0 and 2:2, respectively.

Similarly, alizarin red staining and semi-quantitative analysis also demonstrated that the co-grafted surfaces (i.e., 3:1 and 2:2) could significantly enhance extracellular matrix mineralization compared to controls and mono-grated ones, especially at the feeding ratio of 3:1 was better than that of others (Fig. 3A and C). Therefore, the osteoinductivity of different surfaces showed a DBCO-BMP-2 feeding-dependent manner; sufficient BMP-2 content (no less than 50%) was critical for osteogenesis under the challenging conditions.

QPCR was performed to further evaluate the osteodifferentiation of BMSCs on different modified surfaces at each time point. RUNX2 and Osterix are two key transcription factors necessary for early osteoblast differentiation. Consistent to the ALP and AR staining, the mRNA expression of RUNX2 and Osterix on the dual-functionalized surfaces at the feeding ratio of 3:1 was significantly higher compared to the others at day 3, further indicating the enhanced osteoinductivity of co-grafted Ti surface at the early stage (Fig. 3D and E). The mRNA expressions of ALP and COL1A1 were also the highest in the co-grafted group (3:1)

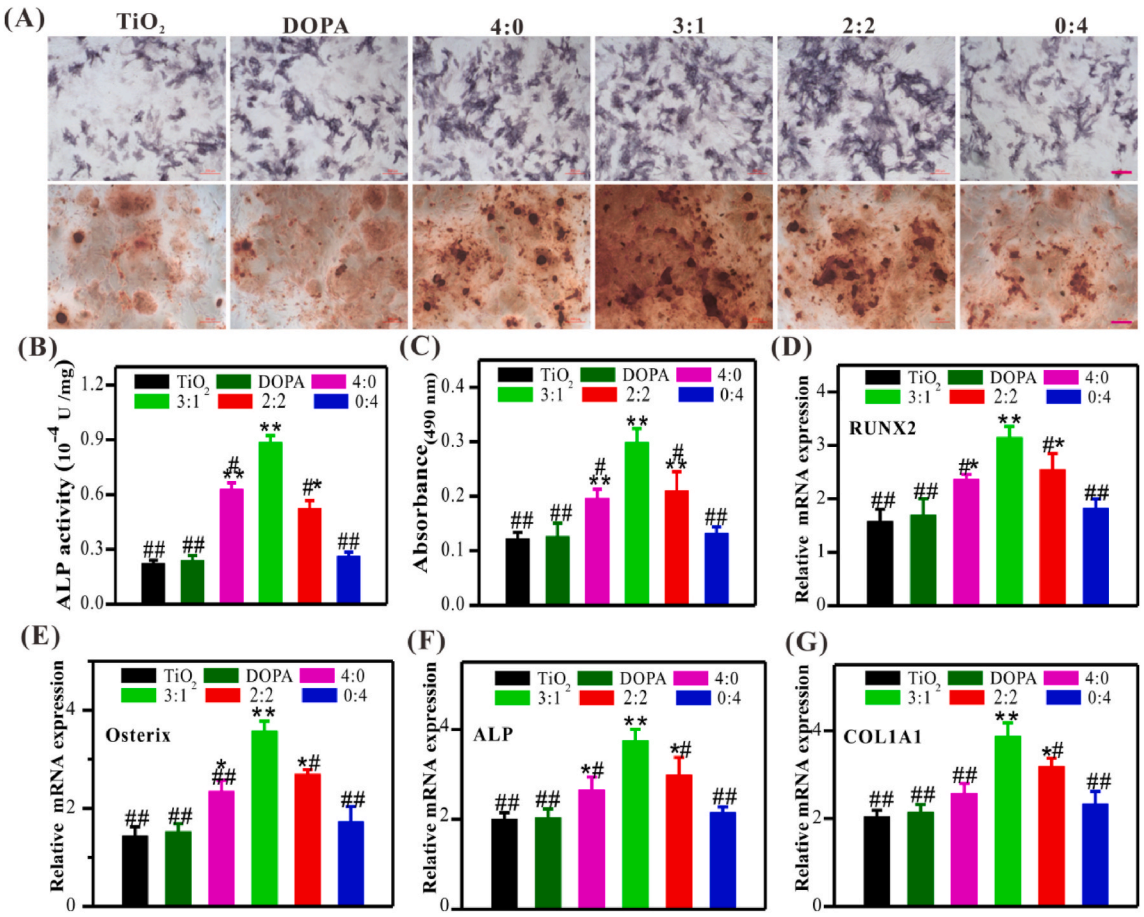

Fig. 3. Osteodifferentiation of BMSCs on different modified TiO_2 substrates. (A) Representative images of ALP and Alizarin Red S staining (Scale bar = 100 μm). (B) Quantitative analysis of ALP activity. (C) Quantitative analysis of Alizarin Red S staining. (D–G) Relative mRNA expression of RUNX2 (D), Osterix (E), ALP (F), and COL1A1 (G). Significant differences were indicated by *p < 0.05 or **p < 0.01 compared with bare TiO2 surface, and #p < 0.05 or ##p < 0.01 compared with the DBCO-BMP-2/DBCO-RGD co-grafted (3:1) surface (n = 3). (For interpretation of the references to colour in this figure legend, the reader is referred to the Web version of this article.)

among all groups after 7 days (Fig. 3F and G). These results jointly demonstrated that BMP-2 and RGD had synergistic effects in capturing BMSCs and inducing their osteodifferentiation at the desired feeding ratio of 3:1.

Then, we further investigated the mechanism of the synergistic effect of the combined application of BMP-2 and RGD. It should be noted that although the surface grafted with RGD alone (4:0) had weak osteoinductivity, the RGD motif on the co-grafted surface also played an indispensable role for osteodifferentiation, which may be due to the interaction of RGD-integrin αvβ3 could enhance the activation of BMPR/Smad signaling pathway. According to the outstanding performance on ALP activity and matrix mineralization, only the co-grafted surface with the feeding ratio of 3:1 was used for subsequent studies. As shown in Fig. 4A–E, the combined use of BMP-2 and RGD could dramatically enhance the activation of the BMPR/Smad signaling pathway after 24 h of incubation. Semi-quantitative analysis showed that the expressions of BMPR/Smad signal pathway-related proteins, including BMPRII, phosphorylated Smad1/5/8 (pSmad1/5/8), Smad4, and BMP-2, on the BMP-2/RGD co-grafted surface were significantly higher compared to the bare TiO_2, RGD mono-grafted, and BMP-2 mono-grafted TiO_2 surfaces, indicating that RGD could enhance the osteoinductivity of BMP-2. To sum up, at the feed ratio of 3:1, BMP-2/RGD co-grafted Ti surface could promote BMSCs adhesion and osteodifferentiation, which were necessary for early osteogenesis and osseointegration *in vivo*.

3.5. Macrophage polarization in vitro and in vivo

At the early stage after implantation, peri-implantitis is a great challenge for osseointegration, especially in the case of osteoporosis, senile edentulous and rheumatoid arthritis, etc [44]. Encouragingly, BMP-2 as an influential osteoinductive factor also encompasses the immunomodulatory capacity [33,34]. Once biomaterials are implanted *in vivo*, the status of macrophages is crucial to the outcome, while classical (M1) is favorable for pro-inflammation and alternative (M2) for anti-inflammation and tissue regeneration [45]. Thus, we further investigated the immunomodulatory capacity of different TiO_2 surfaces by examining the polarization of macrophages. To imitate a chronic inflammatory environment upon clinically osteoporotic conditions, medium containing half dose-effect concentration of LPS and IFN-γ were applied to induce the polarization of M1 or M2 macrophages, respectively.

According to the most superior effects of different surfaces on BMSCs adhesion and osteodifferentiation, the co-grafted surfaces with the feeding ratio of 3:1 were selected. All peptide-grafted surfaces showed a significant decrease of M1 phenotypic macrophage ($CD68^+CD86^+$) compared with the bare TiO_2 in the presence of LPS and IFN-γ (Fig. 5A–C). Comfortingly, upon the grafting of DBCO-BMP-2 (i.e., BMP-2 and RGD+BMP-2 groups) could significantly suppress the M1 polarization. The percentage of M1 macrophages on the dual-functionalized surfaces (RGD+BMP-2) showed a decrease of nearly 33.2% compared to the bare TiO_2 surface. In the absence of DBCO-BMP-2 grafting, the

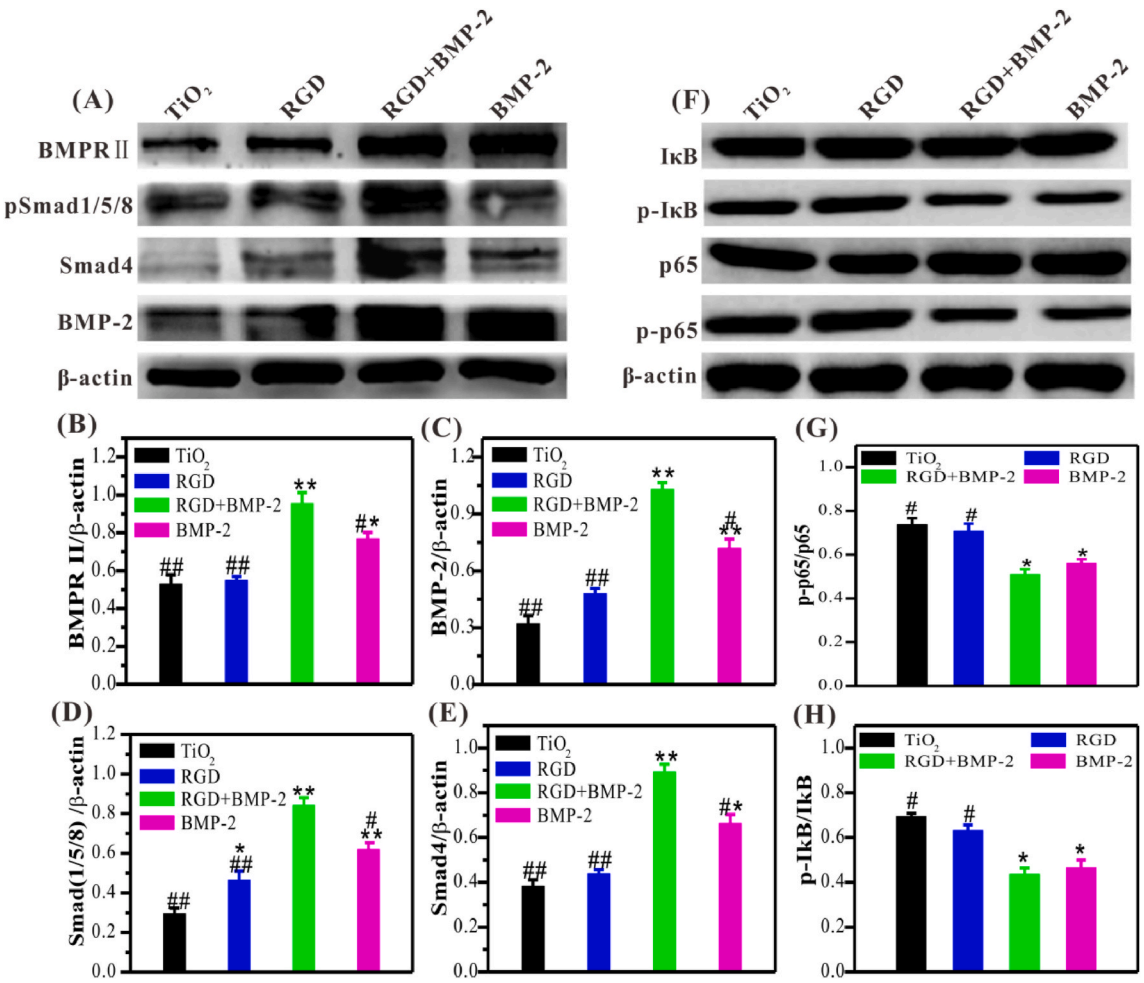

Fig. 4. Western blotting of BMPR/Smad1/5/8 signaling in BMSCs and NF-κB signaling in macrophages. (A) Representative images of western blotting and (B–E) semi-quantitative analysis of the expression of BMPRII, pSmad1/5/8, Smad4, and BMP-2 in BMSCs. (F) Representative images of western blotting and semi-quantitative analysis (G, H) of the expression of phosphorylated IκB and p65 (pIκB and p-p65) in macrophages (under pro-inflammatory conditions). Significant differences were indicated by *p < 0.05 or **p < 0.01 compared with bare TiO2 surfaces, and #p < 0.05 or ##p < 0.01 compared with the dual-functionalized surfaces (n = 3).

percentage of M1 macrophages on the only RGD-grafted surfaces experienced a certain decrease but showed no significant differences compared to bare TiO_2. In contrast, only the BMP-2-grafted surface showed a significant decrease of M1 macrophages, but there was no significant difference compared with the dual-functionalized surface. Remarkably, BMP-2-grafted surface increased M2 phenotype ($CD68^+CD206^+$) population statistically. These results jointly demonstrated that the dual-functionalized TiO_2 surfaces could modulate the transition of macrophages from the pro-inflammatory M1 phenotype to the anti-inflammatory M2 phenotype, which mainly depends on BMP-2 peptide.

M1 macrophages induce local inflammation by secreting TNF-α and IL-1β, while M2 macrophages alleviate inflammation and facilitate osteogenesis by secreting IL-10, VEGF and TGF-β1, etc [45]. As expected, ELISA results showed that on the dual-functionalized surface, the expression of inflammatory factors (IL-1β, TNF-α) in macrophages decreased dramatically (Fig. 5D and E), while anti-inflammatory factor (IL-10) and angiogenic factor (VEGF) increased significantly (Fig. 5F and G), which was consistent with FACS. The enhanced expression of IL-10 and VEGF could also indirectly accelerate osteogenesis via alleviating inflammation and enhancing angiogenesis, indicating a positive feedback loop involving macrophage-mediated osteogenesis. Similarly, qPCR also showed that BMP-2-containing surfaces dramatically diminished the expression of M1 macrophage-specific genes (iNOS, IL-β and TNF-α,) (Supplementary Fig. S2A), but up-regulated the expression of M2 macrophage-related genes (Arg-1, IL-10 and TGF-β1) (Fig. S2B), suggesting that the dual-functionalized surface has a positive immunomodulatory effect under inflammatory condition and shift M1 to M2.

BMP-2 affects many cellular processes by activating the BMPR/Smad1/5/8 signaling pathway, but its specific mechanism for regulating the polarization of macrophages is still unclear. Notably, the NF-κB signaling pathway affects the function of many immune cells and inflammatory reactions in the immune system [44]. Thus, we further detected the expression of two key transcription factors in the NF-κB signaling pathway by western blotting, including phosphorylated p65 and IκB (p-p65 and *p*-IκB). As shown in Fig. 4F–H, the expression of p-p65 and *p*-IκB in macrophages cultured on the BMP-2-containing surfaces was significantly inhibited under the inflammatory conditions, which may be the feedback regulation leading to the decrease of M1 macrophages.

We then subsequently implanted the biomimetic peptide-modified TiO_2 substrates into the osteoporotic rats to check its regulatory effect on macrophages under challenging conditions. As shown in Fig. 6A–C, the dual-functionalized TiO_2 substrates accelerated a significant increase of M2 macrophages, whereas a decrease of M1 macrophage, suggesting that it had the function of inhibiting local inflammatory reaction *in vivo*. The polarization pattern induced by bare TiO_2 substrate was mainly characterized by the significant increase of M1

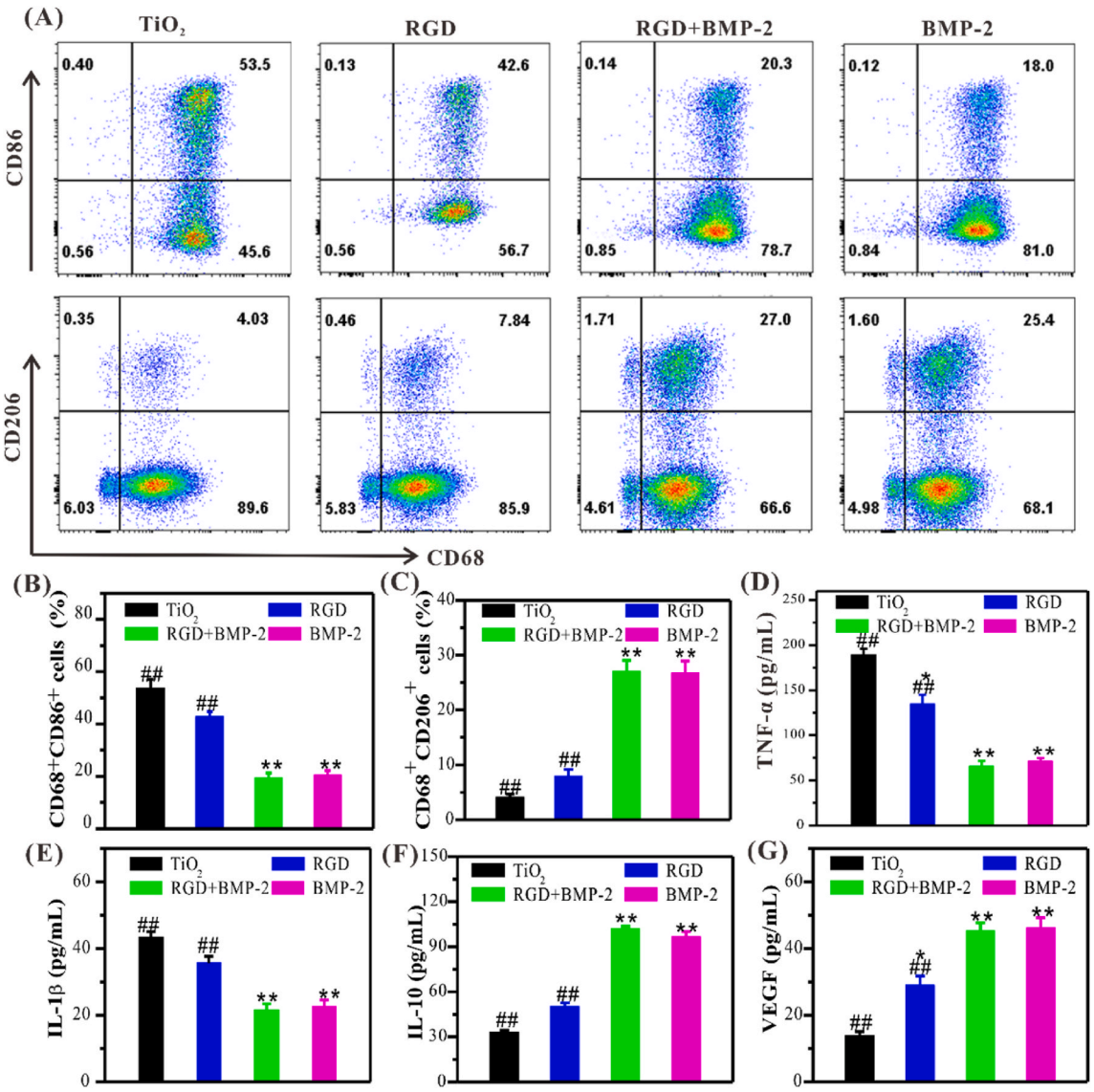

Fig. 5. Characterization of macrophages on different TiO_2 surfaces *in vitro*. (A) FACS analysis of M1 ($CD68^+CD86^+$) and M2 ($CD68^+CD206^+$) phenotypic macrophage. (B, C) Quantitative analysis of M1 or M2 macrophages. (D, E) Pro-inflammatory factors secreted by macrophages on different modified TiO_2 surfaces. (F, G) Anti-inflammatory (IL-10) and angiogenic (VEGF) factors secreted by macrophages on different modified TiO_2 surfaces. Significant differences were indicated by *p < 0.05 or **p < 0.01 compared with bare TiO2 surfaces, and #p < 0.05 or ##p < 0.01 compared with the dual-functionalized surfaces (n = 3).

macrophages, which may be related to the apparent inflammatory reaction at the implantation site. Thus, at the feeding ratio of 3:1 (BMP-2/RGD), the dual-functionalized surfaces were the most superior, with excellent BMSCs adhesion and osteodifferentiation, as well as inflammation suppression, might provide a material-friendly microenvironment to enhance osteogenesis and osseointegration.

3.6. *In vivo* osteogenesis and osseointegration

Undoubtedly, the dual-functionalized surfaces showed superior cell anchoring and osteoinductive capacities as well as inflammation suppression, which would be conducive to facilitate early osteogenesis and osseointegration, especially under clinically challenging conditions. Then, we implanted the Ti-based screws with different modifications into the femoral condyles of osteoporotic rats to assess the potential efficiency for early osteogenesis and osseointegration. To protect the peptide-coatings on the screw surfaces, a drill with a diameter between the screw groove and the convex thread was chosen. Our previous studies have revealed that this strategy can efficiently preserve the peptide-coatings after the implantation, which is a prerequisite for investigating the performance of functionalized screws *in vivo*[24].

After 8 weeks of implantation, the implanted Ti screws with the femoral condyles were harvested as a whole, and then the histological staining, micro CT scanning, and pull-out test were performed to evaluate the osteogenesis and osseointegration. Histological staining morphometric analysis and the bone-implant contact (BIC) determined by the percentage of the bone-implant apposition is the most direct evidence for evaluating osseointegration. As shown in Fig. 6D and E, the dual-functional Ti screws exhibited the best osteogenesis (blue staining), whereas there was the less neo-bone formation on the bare or single RGD or BMP-2-grafted Ti screws surfaces, and the bare Ti screws were the worst. Although there was feeble bone mineral deposition on the surfaces of control and single peptide-grafted screws, which was dispersive and not compact. The bone-implant contact (BIC) is the most intuitive attribute to evaluate osseointegration. Quantitative analysis showed that the BIC of dual-functionalized titanium screws (71.37 ± 5.58%) was nearly 2.32, 1.86, and 1.40 times as that of bare Ti screws (30.71 ± 3.37%), single RGD (39.08 ± 2.06%) or single BMP-2-grafted screws

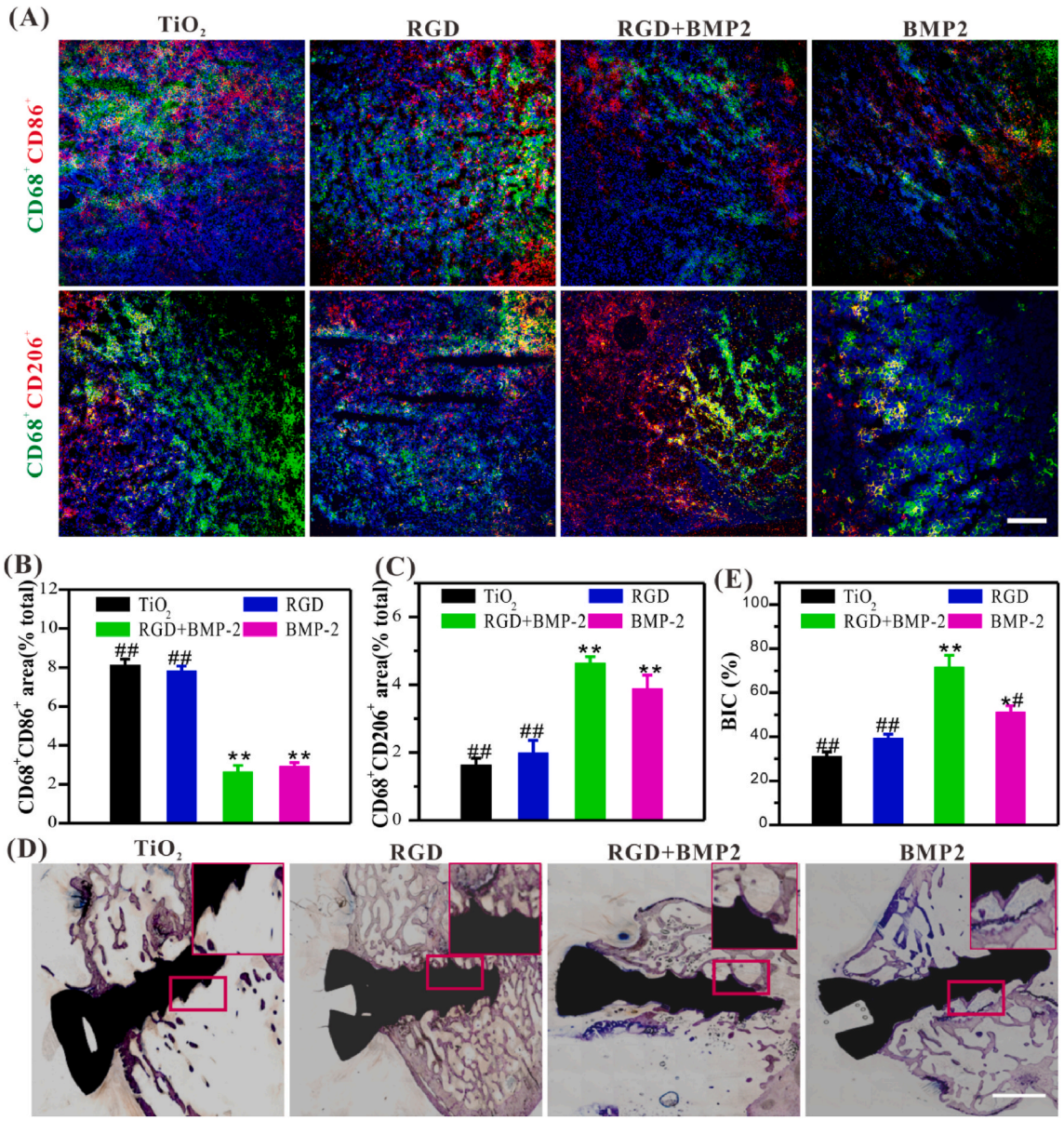

Fig. 6. Histological analysis of the immunomodulatory and osteoinductive capacities of functionalized Ti-based materials *in vivo*. (A) Representative immunofluorescence images of different modified TiO_2 substrates regulating macrophage polarization in osteoporotic rats (Scale bar = 50 μm). (B, C) Quantitative analysis of the polarization of macrophages *in vivo*. (D) Representative histological images of Ti-based screws stained with toluidine blue (Scale bar = 50 μm). (E) The average histomorphometric values of bone-implant contact (BIC). Significant differences were indicated by *p < 0.05 or **p < 0.01 compared with bare TiO2 surfaces, and #p < 0.05 or ##*p* < 0.01 compared with the dual-functionalized Ti-based materials (n = 3). (For interpretation of the references to colour in this figure legend, the reader is referred to the Web version of this article.)

(50.92 ± 3.16%), respectively, definitely demonstrating the excellent osseointegration on the dual-functionalized Ti screws.

As expected, micro CT scanning images clearly showed that the surfaces of dual-functionalized screws were tightly wrapped with the continuous bone mineral layer, demonstrating that there was significant neo-bone formation (Fig. 7A and B). Under the same scanning threshold and VOI, the percentage of the BV/TV of dual-functionalized titanium screws was the highest, which was consistent with the results of *in vitro* osteogenic differentiation. Quantification showed that a nearly 2.87-fold increase of BV/TV in the dual-functionalized group (12.61 ± 0.43%) compared to the bare screws group (4.39 ± 0.0.31%). Moreover, The BV/TV of the dual-functionalized group was 2.03 and 1.47-fold that of the single peptide RGD (6.18 ± 0.32%) and BMP-2-grafted (8.57 ± 0.61%) group, respectively. Similarly, the microstructures of trabecular at the peri-implant interface in the co-grafted group exhibited the best bone condition compared with other groups. The significantly enhanced interfacial ossification and excellent bone condition demonstrated that dual-functionalized screws could efficiently accelerate early osteogenesis and osseointegration even under challenging conditions. Tb.N and Tb.Th values of the dual-functionalized group were also significantly higher than that of other groups (Fig. 7C and D), whereas Tb.Pf and Tb.Sp (Fig. 7E and F) were lower. The single RGD or BMP-2-grafted screws also exhibited slight improvement in bone volume and improved newly formed bone condition. These results, from another perspective, demonstrated that the combined use of RGD and BMP-2 peptides are crucial to enhance osteogenesis, especially under challenging conditions. In addition, these results demonstrated that the dual-functionalized screws (BMP-2 and RGD co-grafted screws) with excellent osteogenicity could significantly promote osteogenesis and osseointegration under challenging conditions.

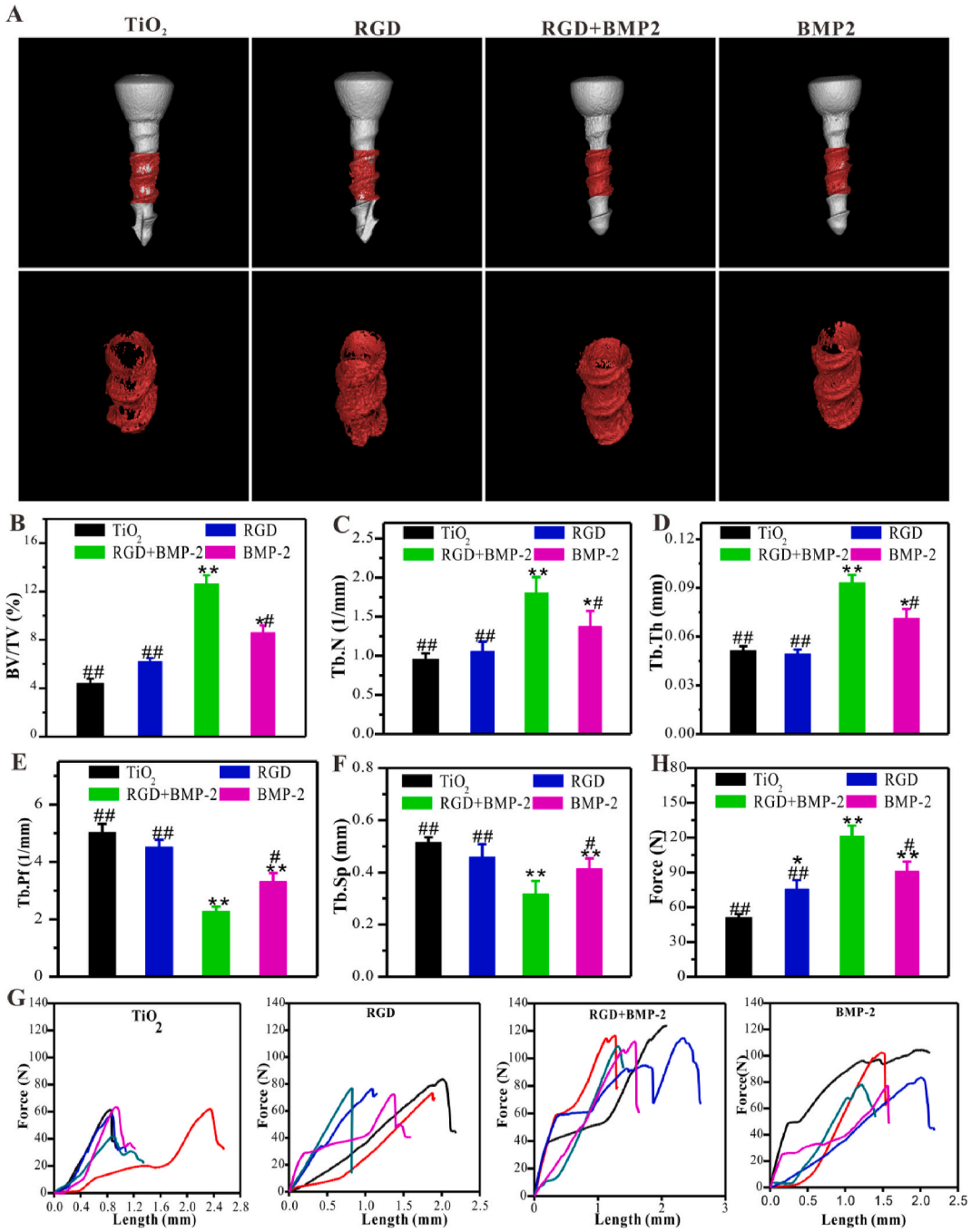

Fig. 7. The dual-functionalized screws exhibited enhanced osteogenesis and mechanical stability *in vivo* compared to the bare screws. (A) Representative micro-CT 3D reconstructed images. (B–F) Quantitative analysis of the peri-implant bone generation (n = 3). (G, H) The results of biomechanical pull-out testing (n = 3). Significant differences were indicated by $^{*}p < 0.05$ or $^{**}p < 0.01$ compared with bare TiO_2 surfaces, and $^{\#}p < 0.05$ or $^{\#\#}p < 0.01$ compared with the dual-functionalized Ti-based materials.

Furthermore, the enhanced osseointegration was confirmed by the biomechanical pull-out test (Fig. 7G and H). The data revealed that the co-grafted screws were stably connected with the surrounding osseous tissues, whereas the weaker connection in the control and mono-grafted groups, probably due to synergistic effects of RGD and BMP-2 on osteogenesis and immunomodulation.

Therefore, we developed a biomimetic approach to introduce a coating of multiple bioactive molecules onto the Ti implant surfaces by combining the mussel-inspired adhesion and bio-orthogonal conjugation. We select two osteogenesis-specific peptides: the BMSCs-anchoring RGD and osteogenic BMP-2, to endow the Ti implants with the desired osteogenicity by shifting the RGD/BMP-2 feeding ratio. Moreover, the above results justified the feasibility of our strategy to inhibit inflammation and generate a favorable microenvironment for BMSCs adhesion and osteodifferentiation onto an optimized co-grafted screw surface *in vivo*. The co-modified surfaces exhibit that the two biomimetic peptides could jointly endow the TiO_2 surfaces with desired properties in a facile and straightforward way, indicating its great potential to improve osseointegration of Ti implants *in vivo*.

4. Conclusion

In conclusion, we have designed a clickable mussel-inspired peptide and two DBCO-capped bioactive peptides for facile decoration of Ti prostheses via robust catechol/TiO2 coordinative interactions and click chemical reaction, which can improve the biocompatibility of Ti implants and endow them with desired bioactivities, including cell anchoring and osteogenicitity. Moreover, by rationally adjusting the grafting ratio of BMP-2 and RGD peptides, it could synergistically achieve M2 shifting and efficient inflammation inhibition; enhance osteogenesis and osseointegration. In addition to the potential application in solving the loosening problem of orthopedic Ti screws, this simple, flexible and rapid modification strategy also has a broad application prospect in the functional modification of metal prostheses used in dentistry, stomatology, and maxillofacial surgery.

CRediT authorship contribution statement

Jie Sun: Conceptualization. **Yingkang Huang:** Conceptualization. **Huan Zhao:** Conceptualization, Methodology, Data curation, Formal analysis, Writing – original draft, Preparation. **Junjie Niu:** Methodology. **Xuwei Ling:** Methodology. **Can Zhu:** Methodology. **Lin Wang:** Methodology, Software, Data curation. **Huilin Yang:** Conceptualization. **Zhilu Yang:** Conceptualization, Methodology, Data curation, Formal analysis, Validation, Writing – review & editing. **Guoqing Pan:** Conceptualization, Methodology, Data curation, Formal analysis, Validation, Writing – review & editing. **Qin Shi:** Conceptualization, Methodology, Data curation, Formal analysis, Validation, Writing – review & editing.

Declaration of competing interest

The authors have no conflicts of interest to disclose in relation to this article.

Acknowledgement

This work was supported by the National Key Research and Development Program of China (2019YFA0112000), the National Natural Science Foundation of China (81972059, 81772358, 21875092), the key R & D programs of Jiangsu Province (BE2019668), China Postdoctoral Science Foundation (2020M671587), Jiangsu Provincial Clinical Orthopedic Center, Priority Academic Program Development of Jiangsu Higher Education Institutions (PAPD), the High-level Talents Research and Development Program of Affiliated Dongguan Hospital, Southern Medical University (K202102).

Appendix A. Supplementary data

Supplementary data to this article can be found online at https://doi.org/10.1016/j.bioactmat.2021.10.003.

References

[1] J. Bai, et al., Biomimetic osteogenic peptide with mussel adhesion and osteoimmunomodulatory functions to ameliorate interfacial osseointegration under chronic inflammation, Biomaterials 255 (2020), 120197, https://doi.org/10.1016/j.biomaterials.2020.120197.
[2] S. Yamada, M. Matsue, J.H. Lee, The reaction of peri-implant tissues to titanium alloy and apatite-coated implants during the healing phase, Nihon Shishubyo Gakkai kaishi 30 (1988) 1021–1031, https://doi.org/10.2329/perio.30.1021.
[3] K.T. Kim, M.Y. Eo, T.T.H. Nguyen, S.M. Kim, General review of titanium toxicity, Int. J. Implant Dent. 5 (2019) 10, https://doi.org/10.1186/s40729-019-0162-x.
[4] E. Jacobi-Gresser, K. Huesker, S. Schütt, Genetic and immunological markers predict titanium implant failure: a retrospective study, Int. J. Oral Maxillofac. Surg. 42 (2013) 537–543, https://doi.org/10.1016/j.ijom.2012.07.018.
[5] P.D. Bianco, P. Ducheyne, J.M. Cuckler, Local accumulation of titanium released from a titanium implant in the absence of wear, J. Biomed. Mater. Res. 31 (1996) 227–234, https://doi.org/10.1002/(sici)1097-4636(199606)31:2<227::Aid-jbm9>3.0.Co;2-p.
[6] X. Guo, et al., Efficient inhibition of wear-debris-induced osteolysis by surface biomimetic engineering of titanium implant with a mussel-derived integrin-targeting peptide, Adv Biosyst 3 (2019), e1800253, https://doi.org/10.1002/adbi.201800253.
[7] M. Becker, et al., Single-cell adhesion of human osteoblasts on plasma-conditioned titanium implant surfaces in vitro, J. Mech. Behav. Biomed. Mater. 109 (2020), 103841, https://doi.org/10.1016/j.jmbbm.2020.103841.
[8] J.C.M. Souza, et al., Nano-scale modification of titanium implant surfaces to enhance osseointegration, Acta Biomater. 94 (2019) 112–131, https://doi.org/10.1016/j.actbio.2019.05.045.
[9] A. Jemat, M.J. Ghazali, M. Razali, Y. Otsuka, Surface modifications and their effects on titanium dental implants, BioMed Res. Int. (2015), 791725, https://doi.org/10.1155/2015/791725, 2015.
[10] J. Chen, et al., Fusion peptide engineered "statically-versatile" titanium implant simultaneously enhancing anti-infection, vascularization and osseointegration, Biomaterials 264 (2021), 120446, https://doi.org/10.1016/j.biomaterials.2020.120446.
[11] H. Haimov, N. Yosupov, G. Pinchasov, G. Juodzbalys, Bone morphogenetic protein coating on titanium implant surface: a systematic review, J. Oral Maxillofac. Res. 8 (2017) e1, https://doi.org/10.5037/jomr.2017.8201.
[12] O.F. Zouani, C. Chollet, B. Guillotin, M.C. Durrieu, Differentiation of pre-osteoblast cells on poly(ethylene terephthalate) grafted with RGD and/or BMPs mimetic peptides, Biomaterials 31 (2010) 8245–8253, https://doi.org/10.1016/j.biomaterials.2010.07.042.
[13] D. Gan, et al., Chitosan/biphasic calcium phosphate scaffolds functionalized with BMP-2-encapsulated nanoparticles and RGD for bone regeneration, J. Biomed. Mater. Res. 106 (2018) 2613–2624, https://doi.org/10.1002/jbm.a.36453.
[14] M.T. Ehrensberger, C.M. Clark, M.K. Canty, E.P. McDermott, Electrochemical methods to enhance osseointegrated prostheses, Biomed. Eng. Lett. 10 (2020) 17–41, https://doi.org/10.1007/s13534-019-00134-8.
[15] Wadhwani, C. P. K., Schoenbaum, T., King, K. E. & Chung, K. H. Techniques to optimize color esthetics, bonding, and peri-implant tissue Health with titanium implant abutments. Comp. Cont. Educ. Dent. 39, 110-119 (2018).
[16] F. Jalali, H. Oveisi, A. Meshkini, Enhanced osteogenesis properties of titanium implant materials by highly uniform mesoporous thin films of hydroxyapatite and titania intermediate layer, J. Mater. Sci. Mater. Med. 31 (2020) 114, https://doi.org/10.1007/s10856-020-06450-1.
[17] L.T. de Jonge, S.C. Leeuwenburgh, J.G. Wolke, J.A. Jansen, Organic-inorganic surface modifications for titanium implant surfaces, Pharmaceut. Res. 25 (2008) 2357–2369, https://doi.org/10.1007/s11095-008-9617-0.
[18] R. Dayer, R. Rizzoli, A. Kaelin, P. Ammann, Low protein intake is associated with impaired titanium implant osseointegration, J. Bone Miner. Res. : Off. J. Am. Soc. Bone Min. Res. 21 (2006) 258–264, https://doi.org/10.1359/jbmr.051009.
[19] Y.S. Park, J.Y. Cho, S.J. Lee, C.I. Hwang, Modified titanium implant as a gateway to the human body: the implant mediated drug delivery system, BioMed Res. Int. (2014), 801358, https://doi.org/10.1155/2014/801358, 2014.
[20] X. Wang, et al., Surface bioengineering of diverse orthopaedic implants with optional functions via bioinspired molecular adhesion and bioorthogonal conjugations, Biomed. Mater. 16 (2021), 024106, https://doi.org/10.1088/1748-605X/abcf02.
[21] Chen, X., Gao, Y., Wang, Y. & Pan, G. Mussel-inspired peptide mimicking: an emerging strategy for surface bioengineering of medical implants. Smart Mater. Med. 2, 26-37, doi:10.1016/j.smaim.2020.10.005(2021).
[22] Y. Hou, X. Deng, C. Xie, Biomaterial surface modification for underwater adhesion, Smart Mater. Med. 1 (2020) 77–91, https://doi.org/10.1016/j.smaim.2020.07.003.
[23] F. Zhang, et al., Mussel-inspired dopamine-Cu(II) coatings for sustained in situ generation of nitric oxide for prevention of stent thrombosis and restenosis, Biomaterials 194 (2019) 117–129, https://doi.org/10.1016/j.biomaterials.2018.12.020.
[24] G. Pan, et al., Biomimetic design of mussel-derived bioactive peptides for dual-functionalization of titanium-based biomaterials, J. Am. Chem. Soc. 138 (2016) 15078–15086, https://doi.org/10.1021/jacs.6b09770.
[25] H. Zhao, et al., Mussel-inspired peptide coatings on titanium implant to improve osseointegration in osteoporotic condition, ACS Biomater. Sci. Eng. 4 (2018) 2505–2515, https://doi.org/10.1021/acsbiomaterials.8b00261.
[26] Z. Yang, et al., Bioclickable and mussel adhesive peptide mimics for engineering vascular stent surfaces, Proc. Natl. Acad. Sci. U.S.A. 117 (2020) 16127–16137, https://doi.org/10.1073/pnas.2003732117.
[27] J. Kim, C.R. Bertozzi, A bioorthogonal reaction of N-oxide and boron reagents, Angew. Chem. 54 (2015) 15777–15781, https://doi.org/10.1002/anie.201508861.
[28] Y. Yang, et al., Endothelium-Mimicking multifunctional coating modified cardiovascular stents via a stepwise metal-catechol-(amine) surface engineering strategy, 2020, Research (Wash D C) (2020), 9203906, https://doi.org/10.34133/2020/9203906.
[29] I. Bilem, et al., RGD and BMP-2 mimetic peptide crosstalk enhances osteogenic commitment of human bone marrow stem cells, Acta Biomater. 36 (2016) 132–142, https://doi.org/10.1016/j.actbio.2016.03.032.
[30] I. Bilem, et al., The spatial patterning of RGD and BMP-2 mimetic peptides at the subcellular scale modulates human mesenchymal stem cells osteogenesis, J. Biomed. Mater. Res. 106 (2018) 959–970, https://doi.org/10.1002/jbm.a.36296.

[31] N.M. Moore, N.J. Lin, N.D. Gallant, M.L. Becker, Synergistic enhancement of human bone marrow stromal cell proliferation and osteogenic differentiation on BMP-2-derived and RGD peptide concentration gradients, Acta Biomater. 7 (2011) 2091–2100, https://doi.org/10.1016/j.actbio.2011.01.019.
[32] J.S. Park, et al., Osteogenic differentiation of human mesenchymal stem cells using RGD-modified BMP-2 coated microspheres, Biomaterials 31 (2010) 6239–6248, https://doi.org/10.1016/j.biomaterials.2010.05.002.
[33] F. Wei, Y. Zhou, J. Wang, C. Liu, Y. Xiao, The immunomodulatory role of BMP-2 on macrophages to accelerate osteogenesis, Tissue Eng. A 24 (2018) 584–594, https://doi.org/10.1089/ten.TEA.2017.0232.
[34] Y. Shu, et al., The immunomodulatory role of sulfated chitosan in BMP-2-mediated bone regeneration, Biomater Sci 6 (2018) 2496–2507, https://doi.org/10.1039/c8bm00701b.
[35] H. Shen, et al., Improved BMP2-CPC-stimulated osteogenesis in vitro and in vivo via modulation of macrophage polarization, Mater Sci Eng C Mater Biol Appl 118 (2021), 111471, https://doi.org/10.1016/j.msec.2020.111471.
[36] E.L. Durham, R. Kishinchand, Z.J. Grey, J.J. Cray, rhBMP2 alone does not induce macrophage polarization towards an increased inflammatory response, Mol. Immunol. 117 (2020) 94–100, https://doi.org/10.1016/j.molimm.2019.10.021.
[37] X. Liu, et al., Immunopolarization-regulated 3D printed-electrospun fibrous scaffolds for bone regeneration, Biomaterials 276 (2021), 121037, https://doi.org/10.1016/j.biomaterials.2021.121037.
[38] H. Qiu, et al., Biomimetic engineering endothelium-like coating on cardiovascular stent through heparin and nitric oxide-generating compound synergistic modification strategy, Biomaterials 207 (2019) 10–22, https://doi.org/10.1016/j.biomaterials.2019.03.033.
[39] M. Li, et al., Rational integration of defense and repair synergy on PEEK osteoimplants via biomimetic peptide clicking strategy, Bioact. Mater. (2021), https://doi.org/10.1016/j.bioactmat.2021.07.002.
[40] X. Zhang, G. Chen, Y. Yu, L. Sun, Y. Zhao, Bioinspired adhesive and antibacterial microneedles for versatile transdermal drug delivery, Research (Wash D C) (2020), 3672120, https://doi.org/10.34133/2020/3672120, 2020.
[41] Sunarso, R. Toita, K. Tsuru, K. Ishikawa, A superhydrophilic titanium implant functionalized by ozone gas modulates bone marrow cell and macrophage responses, J. Mater. Sci. Mater. Med. 27 (2016) 127, https://doi.org/10.1007/s10856-016-5741-2.
[42] E. Gongadze, et al., Adhesion of osteoblasts to a nanorough titanium implant surface, Int. J. Nanomed. 6 (2011) 1801–1816, https://doi.org/10.2147/ijn.S21755.
[43] A. Dusad, et al., Titanium implant with nanostructured zirconia surface promotes maturation of peri-implant bone in osseointegration, Proc. IME H J. Eng. Med. 227 (2013) 510–522, https://doi.org/10.1177/0954411913479300.
[44] M. Chen, et al., Substrate stiffness modulates bone marrow-derived macrophage polarization through NF-kappaB signaling pathway, Bioact Mater 5 (2020) 880–890, https://doi.org/10.1016/j.bioactmat.2020.05.004.
[45] Q. Gu, H. Yang, Q. Shi, Macrophages and bone inflammation, J. Orthopaed.Transl. 10 (2017) 86–93, https://doi.org/10.1016/j.jot.2017.05.002.